Received: 17 July 2022 | Revised: 1 February 2023 | Accepted: 6 February 2023

DOI: 10.1002/eco.2533

RESEARCH ARTICLE

WILEY

Identifying key channel variability functions controlling ecohydraulic conditions using synthetic channel archetypes

Anzy Lee[1] | Belize Lane[1] | Gregory B. Pasternack[2]

[1]Civil and Environmental Engineering, Utah State University, Logan, Utah, USA

[2]Department of Land, Air & Water Resources, University of California Davis, Davis, California, USA

Correspondence
Anzy Lee, Civil and Environmental Engineering, Utah State University, Logan, UT, USA.
Email: anzy.lee@usu.edu

Funding information
California State Water Resources Control Board, Grant/Award Number: 16-062-300; USDA National Institute of Food and Agriculture, Grant/Award Numbers: CA-D-LAW-2243-H, CA-D-LAW-7034-H; Utah Water Research Laboratory, Utah State University

Abstract

Geometric modelling of river channel topography is a method of design synthesis wherein specific 2D geometric elements of river topography, such as the bed profile, cross-sectional shape and channel planform contours, are expressed mathematically in isolation and then combined to produce a 3D heightmap. We utilized the geometric modelling framework to synthesize channel terrains that reveal flow–form–function linkages to investigate what roles variability in bed roughness, thalweg elevation and channel width play in defining hydraulic and ecohydraulic conditions of a channel reach from baseflow to bankfull discharge. To achieve a robust inquiry for a range of settings, this study developed four distinct synthetic channel terrain models for each of three stream reaches of different channel types in the South Fork Eel River in northern coastal California, USA. To test the process-based effects of these diverse terrain synthesis options, we compared the resulting hydraulic patterns and preferred habitat availability for fry/juvenile steelhead trout and coho salmon over a range of discharges. Among thalweg bed undulation, width variation and bed roughness, we found thalweg bed undulation was the key factor affecting the channel ecohydraulic response at baseflow condition. At bankfull condition, thalweg bed elevation had the largest effect in high-order mainstem streams identified by gravel-cobble dominated high width-to-depth, riffle-pool sequences, width variation had the largest effect in mid-order confined channels with gravel-cobble, high width-to-depth ratio with expansions/contractions and bed roughness in low-order streams with low width-to-depth ratio, high-gradient, cobble-boulder and step-pool/cascade channels.

KEYWORDS
channel classification, channel variability functions, ecohydraulic responses, synthetic archetypes

Significance Statement

We created synthetic channel terrains to examine what roles longitudinal variability in bed roughness, thalweg elevation and channel width play in defining hydrualic conditions and habitat suitability of a channel reach for various flow conditions. We found thalweg elevation variation was the key factor characterizing the hydraulic and ecohydraulic conditions at low flows. Our findings can help reduce field surveying efforts by prioritizing the channel variability features that need to be represented. For example, one may only need channel thalweg elevation measurements to generate a high-resolution synthetic terrain capable of reproducing 2D suitable habitat area patterns of sufficient accuracy for some applications.

1 | INTRODUCTION

In fluvial geomorphology, the ability to make specific, incremental changes to channel topography facilitates investigation of flow–form–function linkages. Synthetic river archetypes allow users to alter the geomorphic properties of channels such as pool-riffle sequences (Brown & Pasternack, 2014; Cao et al., 2003; Pasternack et al., 2008; Wohl et al., 1999), geomorphic covariance structures (Brown et al., 2016; Brown & Pasternack, 2017) and channel bed and width undulations (Anim et al., 2019; Lane et al., 2018). Researchers can then explore the effects of simultaneous changes to the flow regime and channel form on fluvial geomorphic processes (e.g. riffle-pool self-maintenance; Brown & Pasternack, 2017) or river ecosystem functions (e.g. salmonid rearing habitat; Lane et al., 2018). Studies on river flow–form–function linkages using archetypal approaches typically involve either (1) manually manipulating surveyed topography (Brown & Pasternack, 2009; Escobar-Arias & Pasternack, 2011; Jackson et al., 2015; Sear & Newson, 2004) or (2) synthesizing a river archetype with user-defined geomorphic attributes (Anim et al., 2019; Cardenas, 2009; Lane et al., 2018; Lee et al., 2020; Trauth et al., 2013). In one example of the former approach, Escobar-Arias and Pasternack (2011) evaluated the gravel-bed riffle functionality for salmonid habitat at several channel cross-sections on the Yuba River, California. They manually modified the high-resolution topography to generate and compare an alternative channel terrain without riffle-pool sequences using a computer-assisted drafting (CAD) program and ArcGIS. Jackson et al. (2015) also altered existing topography to test the role of width in pool-riffle maintenance. This method requires a detailed, site-specific dataset to produce altered channel terrains for a single site. Alternatively, generating synthetic river corridors using geometric functions requires less effort and is exact, compared to artistically manipulating topographic points and contours. This is called 'procedural generation' (Freiknecht & Effelsberg, 2017), and it allows users to precisely isolate, evaluate and adjust any morphological feature or longitudinal variance pattern of interest.

Several studies have successfully utilized the geometric modelling framework to synthesize channel terrains that reveal flow–form–function linkages. Lane et al. (2018) suggested an integrated modelling approach to investigate the effect of river flow and form configurations on ecosystem function performance based on geometric modelling. Anim et al. (2019) explored how alternative channel morphological designs with oscillating topographic variables affect instream ecohydraulic conditions. Their results showed that the ecohydraulic conditions such as hydraulic diversity and refuge habitat were incrementally improved with the addition of natural oscillations to an increasing number of individual topographic variables in a degraded channel. However, the site-specific geomorphic variability features such as bed undulation and width variation in these studies were quite simplistic—relying on a single sinusoidal wave function.

Recent improvements to geometric modelling of synthetic channel archetypes facilitates creation of realistic river channels and enables researchers to tackle a variety of scientific questions that have existed in the field for quite some time but not been systematically analysed. The free, open-source software River Builder (1.2.0) allow users to synthesize complex river channels through its newest functionality to add discrete features, such as steps, waterfalls, dams, bed sills, large and small bed elements and topographic roughness (Pasternack & Zhang, 2021). It also uses signal creation and reconstruction techniques expressing any arbitrary variability functions (e.g. width, thalweg bed elevation and floodplain contours) with a set of sinusoidal waves in the simplest case. For channel features that cannot be replicated with that type of function, the user can also create patterns with six other variability functions alone or in combination: linear, sine-squared, cnoidal, square wave, Perlin and gooseneck. Finally, all of these functions can be applied on a piecewise basis for a fixed length of a reach or to the entire reach. Thus, the capabilities exceed current scientific understanding of fluvial form sufficient to control the software to obtain the best outcome.

One of the scientific challenges to evaluating flow–form–function relationships is to unravel the contribution of channel variability functions that determine the channel type, which in turn has been linked to ecological structure and function of rivers (Hack & Goodlett, 1960; Lane et al., 2017; Smith et al., 1995; Thomson et al., 2001; Vannote & Sweeney, 1980). Here, a channel type refers to a category of stream system morphologies having common landform and channel characteristics such as slope, confinement, substrate properties, sediment supply, width/depth ratio, sinuosity and uniformity of the channel (Rosgen, 1994). For example, in the Rosgen stream classification system, 'Aa+'-type channels are very steep (>10%) with a low width/depth ratio, totally confined and associated with bedrocks and high sediment supply. In contrast, stream type 'C' has a well-developed floodplain with a large width/depth ratio and mild channel slope (<2%) while exhibiting pool-riffle sequences. Lane et al. (2018) and Anim et al. (2019) showed a systematic approach to analyse flow–form–function linkages for distinct channel types. However, the general applicability of their conclusions across different channel reach morphological settings remains unclear as they compared a limited number of sites within similar, simplistic channel types (e.g. plane bed vs. pool riffle).

Key Points

- River archetypes with bed roughness and longitudinally varying baseflow/bankfull flow width and thalweg elevation were made to represent observed rivers.
- Thalweg elevation variation had the largest effect on mimicking natural ecohydraulic responses in more channel types.
- Bed roughness and width variation also could be most important in other channel types.

This study asks which sub-reach channel variability functions among bankfull width variability, thalweg bed elevation variability and bed roughness define hydraulic and ecohydraulic conditions of a channel reach, and how the effect varies with flow conditions. Although there are many other channel features and patterns available to investigate, these are the three most common ones addressed in fluvial geomorphic research. In this study, hydraulic responses are represented by the joint probability distribution of depth and velocity. Ecological responses are defined by discharge-habitat availability curves. We hypothesize that (1) thalweg bed elevation variation is a key factor in describing baseflow or low-flow hydraulic responses for any channel type, because it affects the cross-sectional flow area: an increase in thalweg bed elevation constricts cross-sectional area imposing alternating areas of high velocity, nozzle-like hydraulics at riffles and low velocity backwater hydraulics at pools. We further hypothesize that (2) thalweg bed elevation variation has the largest effect in high-order mainstem streams identified by gravel-cobble, high width-to-depth ratio, riffle-pool sequences, while (3) width variation has the largest effect in intermediate confined channels characterized by gravel-cobble, high width-to-depth ratio with expansions/contractions, and (4) bed roughness has the largest effect in low-order streams where channel topography is characterized by steep, low width-to-depth ratio, cobble-boulder step-pool/cascades for bankfull flow condition. In addition, (5) the synthetic channel scenario that produces the hydraulic conditions most similar to those simulated using surveyed terrain at bankfull condition will also yield comparable aquatic habitat suitability so that hypotheses (2)–(4) are also true for ecohydraulic conditions. The ability to simulate two-dimensional (2D) hydraulic and ecohydraulic conditions and patterns with sufficient accuracy using parsimonious synthetic channel archetypes that capture the essential features of a terrain necessary to simulate ecohydraulic functionality would represent an important step towards simulating channel-to-network-scale geomorphic functions and aquatic habitat conditions within minimal field data requirements.

2 | STUDY BASIN

The 1782 km^2 South Fork Eel River (SFER) catchment is located in coastal northern California, USA. Composed of highly erosive Franciscan geology, the catchment is characterized by high sediment loading in streams (CDFW, 2014). Average annual discharge is 1.64 km^3 (Eel River Forum, 2016), and mean annual rainfall is estimated at 182.88 cm (IFSP, 2016). Like many regions in seasonally arid climates, SFER experiences cool wet winters and warm dry summers, resulting in a highly seasonal flow regime with immense inter-annual variability. In recent years, however, SFER has experienced extended low-flow periods in winter and early spring due to changes in precipitation patterns and surface water diversions and groundwater pumping associated with rural residences, cannabis cultivation, pastures and forage crops as well as municipal water systems (Asarian, 2015). The fluvial geomorphology of SFER can be described as moderately steep tributaries with incised valleys draining into a low gradient mainstem stream (BLM et al., 1996). Stream elevation changes significantly where tributaries cross large resistant rock blocks, draining into a low gradient mainstem (Byrne et al., 2020; CDFW, 2014).

The Eel River watershed historically supported vast populations of now threatened and endangered salmonid species. SFER remains the most productive and important major tributary for salmonids, hosting all three north coast listed salmonids—Chinook, coho and steelhead (BLM, 2001; CWPAP, 2014)—and is the focus of major past and ongoing restoration efforts for coastal salmonids (CWPAP, 2014). While diminishing salmonid populations have many drivers, maintaining or creating suitable habitat conditions for different life stages (e.g. spawning, rearing, adult holding) through streamflow and channel changes remains a major long-term focus of natural resource agencies (Yoshiyama & Moyle, 2010). Salmonids utilize a diverse array of instream habitats and have variable life histories. Accurate representation of suitable habitat versus discharge requires linking stream channel hydraulics over a range of flows, with known habitat suitability criteria (HSC) for the target species and life stages. The California Department of Fish and Wildlife recently developed HSCs for coho and steelhead juvenile rearing habitat based on snorkel surveys collected in an SFER tributary stream. Juvenile rearing is a critical life stage for instream management because, unlike anadromous adults, juvenile salmonids remain in the stream year-round and are thus sensitive to changes in habitat under summer low-flow conditions (CDFW, 2020).

3 | METHODOLOGY

3.1 | Experimental design

It is plausible that with enough procedural elements one can nearly perfectly replicate any existing fluvial terrain. However, this study did not seek to test that concept. We use the term parsimonious to refer to archetypes that attempt to capture the essential features of a terrain just necessary to achieve ecohydraulic functionality (sensu Fenicia et al., 2007; Petrucci & Bonhomme, 2014; Wagener et al., 2001; Yang et al., 2020). There are two values of parsimonious design for river science and management: first, the hope that topographically complex real rivers can be synthesized from explicit equations that can be added or removed to study individual and synergistic effects; second, the hope that a small number of archetypes could serve to capture and represent the essential functionality of a large number of the world's channel types.

To answer the study's scientific question seeking the right parsimonious procedural design elements, we developed four parsimonious synthetic channel archetypes (henceforth *scenarios*) comprising different channel variability functions (Table 1) to replicate each of three channel reaches surveys spanning a diversity of geomorphic channel types (detailed below). All scenarios employed the same reach-average site attributes, so they differ only in their representation of sub-reach-scale geometric variability. Scenario *n0* had no variability functions (termed a 'vanilla

TABLE 1 Baseline starting dimensions and optional topographic variability functions for each synthetic channel scenario.

Synthetic channel scenario	Reach-average baseline dimensions	Bed roughness	Bankfull width variations	Thalweg bed elevation
n0	X			
s0	X	X		
s1	X		X	
s2	X			X

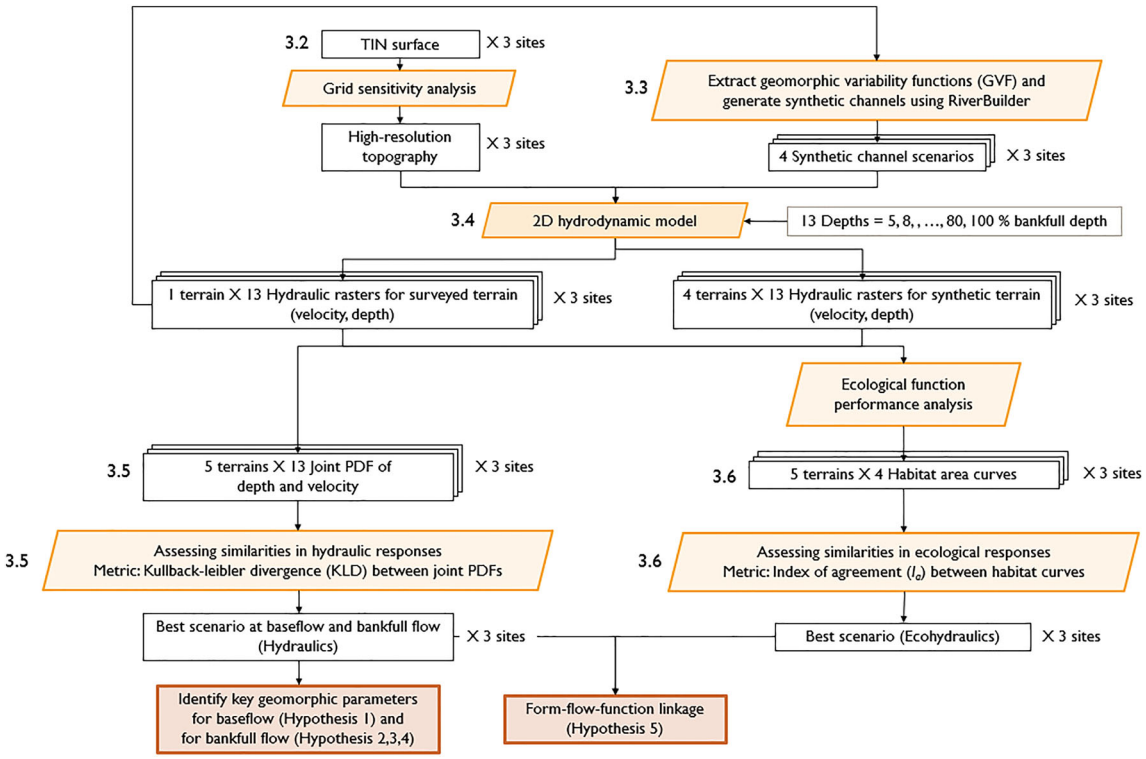

FIGURE 1 Workflow of channel design and ecohydraulic analysis framework.

channel' archetype); scenarios *s0*, *s1* and *s2* each included only one variability function. To test our hypotheses, for each site, we identified the best synthetic channel scenario (i.e. specific combination of parsimonious channel variability functions) and the associated variability function in terms of their ability to reproduce survey-based hydraulic and ecohydraulic conditions (henceforth baseline scenario). The detailed procedure is as follows.

Under each scenario, we evaluated the spatial patterns and probability distributions of depth and velocity to represent hydraulic responses. We also assessed aquatic habitat suitability for fry and juvenile steelhead trout and coho salmon across various flow–form scenarios. For each site, we determined the best-performing scenario that yielded the smallest deviation in hydraulic and ecological responses compared to those of the baseline scenario to test the last hypothesis. Best-performing in this case does not mean to replicate the topography of a real site as accurately as possible, but instead to replicate the hydraulic and ecohydraulic conditions of the real channel terrain (baseline scenario) across a range of river stages with the least synthetic design components necessary to achieve that. In other words, best scenario seeks a parsimonious geometric model structure.

We developed a transparent, repeatable framework to generate synthetic channels to simulate surveyed terrains in terms of channel morphology (form), hydraulic conditions (flow) and aquatic habitat suitability (function) and evaluate archetype performance (Figure 1). For each site, a TIN surface was generated based on the total station survey data. The TIN surface was then converted to a raster digital elevation model (DEM) with a grid size determined by sensitivity analysis (Section 3.2). From the DEM and water surface elevation (WSE) field at bankfull flow, a set of geomorphic variability functions (e.g. bankfull width or thalweg bed undulation) and reach-average parameters (e.g. slope, minimum depth for inner channel lateral and vertical offsets, etc.) were extracted (Section 3.3). Input parameters for each synthetic channel scenario were determined based on the information extracted. Width variations and thalweg bed elevation were approximated by the summation of multiple sinusoidal waves, as detailed below. Bed roughness was represented by a random Perlin noise function added to the elevation of the inner channel bed. When

a sub-reach variability function was not considered, the value was set to zero (e.g. bed roughness, thalweg bed undulation) or a reach-average value (e.g. width). Four different types of synthetic terrains were then created using River Builder 1.2 (available at https://github.com/RiverBuilder/RiverBuilder).

For each surveyed site, 2D hydrodynamic simulation was performed for the baseline scenario topography and its four associated synthetic channel scenarios for a set of flows to obtain the velocity, depth and WSE field along the reach (Section 3.4). Using the depth and velocity rasters, we calculated the probability and cumulative distribution functions of these hydraulic variables to represent hydraulic responses (Section 3.5). For each site, the synthetic terrain scenario that generated the smallest deviation compared to the baseline scenario was selected, and the corresponding geomorphic variability function was identified as a key factor characterizing hydraulic responses. Finally, we compared the predicted ecological function performance of the baseline scenario and synthetic channel scenario terrains by carrying out habitat suitability analysis (Section 3.6). We also evaluated whether the selected synthetic channel scenario resulted in comparable ecological responses to the baseline scenario.

3.2 | Baseline channel terrains

This study sought to create parsimonious synthetic terrains representing the range of channel morphologies exhibited in the SFER catchment. Byrne et al. (2020) identified seven distinct channel types in the catchment among 97 sample reaches characterized with transect-based geomorphic field surveys and classified using multivariate, statistical clustering. Different channel types exhibit distinct geomorphic properties such as bankfull width to depth ratio, contributing area, grain size, coefficient of variation of bankfull depth and valley confinement.

In this study, we regrouped seven regional channel types into three generic channel types, which were low-order (e.g. headwater streams), intermediate and high-order streams (e.g. mainstem), and selected three channel reaches to survey at high resolution to serve as baseline scenarios for each channel type (Table 2.). SFE 322 represents high-order streams identified by gravel-cobble, high width-to-depth, riffle-pool sequences. SFE 25 represents intermediate confined uniform channels with gravel-cobble beds and high width-to-depth ratio. SFE 209 exemplifies low-order streams characterized by low width-to-depth, high-gradient, cobble-boulder and step-pool/cascade. We only considered confined channels as the SFER catchment is dominated by confined settings throughout the region (Guillon et al., 2019).

For each study reach (Table 2), a feature-based topo-bathymetric survey was performed in summer 2018 according to the Columbia Habitat Monitoring Program protocol (chapter 5 of Bouwes et al., 2011). A Leica TPS1200 robotic total station measured bed positions in a relative, local coordinate system. A higher point density was used where topography was steeper. Points mapped key landforms, breaklines (e.g. bank top, bank toe and other local slope breaks) and the thalweg profile. The average sampling density across sites was 0.31 points per m^2. Surveying accuracy was assessed using control network checks. Horizontal and vertical deviations typically ranged from 0.005 to 0.02 m, which is typical for local coordinate systems used over a small area and significantly smaller than the natural topographic uncertainty induced by the coarse bed material present at these mountain river sites.

A DEM was constructed for each study reach using the surveyed topographic points in ArcGIS Pro 2.6.0. The four iterative stages of DEM development as described by French and Clifford (2000) were implemented: interpolation, visualization, editing and augmentation. First, survey data were interpolated, and a surface defined respecting breaklines. Next, the surface was visualized as a map and edited to remove obvious interpolation errors. The revised surface was visually verified against site photos and the experiences of the survey crew to check for poorly represented areas in the DEM. Further iteration was done as needed. Each final DEM was generated as a triangular irregular network (TIN) respecting breaklines. TIN surfaces served as the baseline for synthetic terrain analysis and were converted into grids for hydrodynamic modelling.

3.3 | Generating synthetic river archetypes using river builder

In this section, the steps of generating synthetic rivers using River Builder (RB) are described. According to the Pasternack and Zhang (2021) RB user's manual, the software is set up to receive reach-average metrics as well as the parameters necessary to procedurally generate variability functions and discrete objects. However, it is up to the user to know which and how many functions and objects they

TABLE 2 SFER feature-based survey channel reach attributes.

Reach ID	Channel type	# of survey points	2D TIN surface area (m)	Overall point density(points/m^2)
SFE 322	High-order mainstem streams with gravel-cobble, high width-to-depth ratio, riffle-pool sequences	2514	19,159.77	0.13
SFE 25	Intermediate confined uniform channels with gravel-cobble, high width-to-depth ratio	1236	14,220.46	0.09
SFE 209	Low-order streams with low width-to-depth, high-gradient, cobble-boulder and step-pool/cascade	1060	1488.65	0.71

want to use and with what parameter values. Therefore, new research was needed to be able to 'reverse-engineer' real terrains to obtain RB inputs suitable for synthesizing an archetype from any given terrain. The novel procedure consists of (1) conceptualizing a river corridor in terms of its essential elements and scales on the basis of ecological and geomorphic goals and (2) parameterizing RB geometric functions based on 'reverse engineering' of baseline scenario features obtained from 2D hydrodynamic simulations.

For this study, inputs were extracted from 2D model simulations instead of from the DEM alone, because the goal was to accurately represent the patterning of bankfull width and depth spatial series, which are hydraulic features, not topographic ones. Given a nonuniform channel with an undulating riverbed, it is more accurate to extract flow-dependent channel features from 2D model outputs than through pure geometric analysis of a DEM. The latter could be done using the procedure explained in Pasternack et al. (2021) when no 2D model is available or desired.

3.3.1 | Conceptualization of river corridor and river builder inputs

Each synthetic river channel generated using RB for this study was composed of an inner channel, lateral slope breaks (e.g. outer channel planform contours) and valley walls. Domain parameters such as valley slope, channel length and centreline planform function define the overall shape, sinuosity and extent of the channel and remained unchanged across terrain scenarios for a given site. In RB, the inner channel is defined as the innermost conduit of water in the river valley. While objects and bed roughness patterns may be placed inside the inner channel, there is no smaller geometric channel shape or individual planform contour that can be nested within it. A user can choose to set the inner channel as a baseflow channel, a bankfull channel, or whatever else suits their need.

Inner channel properties were assigned differently depending on the sub-reach variability functions considered in each scenario (Table 3). If width variation was considered (Scenario *s1*), then the inner channel lateral offset minimum [A4] was set to the minimum bankfull width and the inner bank function [A6] was the bankfull width series. Note that the letter and number in square brackets indicate the column and row in Table 3. Otherwise, the inner channel lateral offset minimum was set to the average bankfull width while having no width variation. The same logic applies to thalweg bed undulation, which affects [A5] and [A7]. If bed roughness was chosen for the archetype, then the bed roughness height was determined by expert judgement; otherwise, it was set to zero. Floodplain topography is governed by outer channel properties in RB, including left/right minimum lateral offset and its height offset.

TABLE 3 Geometric variables used to generate river archetype using river builder software and the corresponding metrics estimated from baseline scenarios. Asterisk indicates a sub-reach topographic variability function.

	No.	[A] Input parameters for river builder	[B] Variables measured from baseline scenarios
Domain parameters	[1]	Valley slope	Slope of thalweg elevation
	[2]	Length	Straight length of the channel
	[3]	Centreline function	Centreline amplitude, frequency, phase
Inner channel properties	[4]	Inner channel lateral offset min.	If width variation was chosen, Min. Width at bankfull
			Else, Avg. width at bankfull
	[5]	Inner channel depth min.	If thalweg bed undulation was chosen, Min. Of water depth at thalweg
			Else, Avg. of water depth at thalweg
	[6]	Left/right inner bank function*	If width variation was chosen, (width series at bankfull)/2
			Else, none
	[7]	Thalweg elevation*	If thalweg bed undulation was chosen, Thalweg bed elevation
			Else, none
	[8]	Cross-sectional shape	Determined by expert judgement
	[9]	Perlin bed roughness*	If bed roughness was chosen, Bed roughness height will be determined by expert judgement
			Else, none
Outer channel properties	[10]	Left/right 1st outer bank lateral offset min.	(min. Floodplain width)/2
	[11]	Left/right 1st outer bank height offset	Average of (floodplain elevation - Thalweg elevation)
	[12]	Left/right 1st outer bank function	None

3.3.2 | Reverse-engineering geometric functions from baseline scenarios

The procedure to reverse engineering a parsimonious geometric function from spatial series of any longitudinal feature of a river corridor was as follows: (1) generate 2D pathways (e.g. straight valley centreline, thalweg polyline and thalweg bed undulation) from the baseline scenario of a real terrain and its bankfull discharge 2D model simulation, (2) discretize 2D pathways into a spatial series, (3) calculate valley slope and channel length, (4) specify minimum offset values, and (5) convert a spatial series into oscillatory components. More details are provided in Supporting Information (pp. 2–4).

3.3.3 | Cross-sectional shape and bed roughness

Decisions on cross-sectional shape and bed roughness height were made using expert judgement as follows and to take advantage of RB's capabilities. The cross-sectional shape and bed roughness height applied for each SFE site are listed in Table S1. If the thalweg notably deviated from the centreline of the channel, the cross-sectional shape was set to asymmetrical U-shape (AU); otherwise, a symmetrical U-shape (SU) was used. Note that (1) for SU, the thalweg is identical to the centreline, while for AU the thalweg is dictated by the curvature equation in RB, which makes it deviate from the centreline, and (2) the lateral/vertical offsets and functions were symmetrically assigned.

Bed roughness height was estimated using the particle class size data collected from 97 transect-based geomorphic field surveys. Roughness height was set to 1 m if the percentage of particles exceeding 1 m diameter was >20%. Otherwise, it was set to 0.5 m if the percentage of particles exceeding 0.2 m diameter was >10%. If neither of these conditions were met, then it was set to 0 m.

3.4 | Hydrodynamic modelling

2D hydrodynamic modelling was used to (1) obtain baseline scenario bankfull wetted area polygons from which width spatial series were extracted, (2) create the XY thalweg pathway for each baseline scenario and obtain bed elevation and water depth spatial series along it and (3) simulate depth and velocity rasters of surveyed and synthetic channel terrains over a range of discharges. For the baseline scenarios, TIN surfaces generated from total station surveys (Section 3.2) were converted into raster DEMs for input to a hydrodynamic model. A sensitivity analysis on DEM grid size was conducted by comparing the actual surface area of the raster area with the area of the TIN area (Figure S4). The appropriate grid size was selected as the maximum grid size ensuring the ratio of raster area to TIN area was larger than 0.95 but kept ≤1 m. The mesh resolution for hydrodynamic modelling was set to the grid size used to convert a TIN surface to DEM (Table S1).

TUFLOW 2020-01-AB GPU was used to simulate the spatial patterns of depth and velocity for given channel terrains and flow conditions. TUFLOW is a commercial 2D hydrodynamic model developed by BMT WBM Pty Ltd (https://www.tuflow.com/). It is very stable and computationally efficient and can be programmed for automated batching of numerous simulations (Syme, 2001). Table S1 lists the hydrodynamic model inputs including hydraulic condition (e.g. bankfull discharge) and geomorphic parameters (e.g. slope, Manning's n) for the surveyed and synthetic terrains. Manning's n values were estimated for baseline scenarios based on the USGS photo library (https://wwwrcamnl.wr.usgs.gov/sws/fieldmethods/Indirects/nvalues/index.htm) and past 2D model calibration experience.

For boundary conditions, 13 upstream discharges and their corresponding downstream water stages were determined as follows. For the upstream boundary condition, discharges (Q_i) were evaluated for each terrain ranging from 5% to 100% of bankfull depth. Bankfull depth was estimated as the vertical distance between the thalweg bed elevation and the elevation of the lateral bank slope break at the most upstream riffle crest of the channel reach. Since rating curves were not available at most sites, corresponding upstream discharges were calculated using Manning's equation. For the downstream boundary condition (e.g. outlet), we numerically solved Manning's equation for the downstream water depth for a given discharge.

3.5 | Evaluating hydraulic conditions

Joint frequency distributions of hydraulic variables were used to characterize the general hydraulic patterns of each hydrodynamic model run and as input to the habitat suitability analysis. Depth and velocity rasters were obtained from model runs for all channel scenarios (one surveyed and four synthetic) across all discharges. Joint probability distribution functions (PDFs) of depth and velocity were generated, with bin size determined using Freedman–Diaconis estimator, which accounts for a non-Gaussian distribution from its interquartile range (Freedman & Diaconis, 1981). The Kullback–Leibler divergence (KLD or D_{KL}) of the joint PDFs of the surveyed (p) and synthesized (q) terrains was used to evaluate the dissimilarity in hydraulic responses associated with the synthetic terrain (Equation 1) (Kullback & Leibler, 1951).

$$D_{KL}\left(P\middle\|Q\right) = \int_{-\infty}^{\infty}\int_{-\infty}^{\infty} p(x,y)\log\log\left(\frac{p(x,y)}{q(x,y)}\right)dxdy \quad (1)$$

where x, y denote depth and velocity and $p(x, y)$ and $q(x, y)$ are the probability densities of surveyed and synthetic terrains, respectively. The best-performing archetype was indicated by the lowest KLD value when comparing each archetype to the baseline scenario. KLDs for each channel scenario were calculated for baseflow and bankfull conditions, where baseflow condition was manually identified for each site (5%, 12% and 10% bankfull depth for SFE 322, 25 and 209, respectively) and bankfull condition corresponded to 100% bankfull depth.

3.6 | Evaluating ecohydraulic conditions

Physical habitat suitability was evaluated to determine how much suitable habitat area was available for fry and juvenile steelhead trout and coho salmon for a range of discharges. In this study, we used a set of habitat suitability curves (HSC) developed for SFER catchment to represent the observed organism preference for particular hydraulic habitat conditions (CDFW, 2020; Figure S5).

The ecohydraulics module in the open-source RiverArchitect software (Schwindt et al., 2020) was used to produce habitat suitability index (*HSI*) rasters from input rasters of depth (HSI_d) and velocity (HSI_v), for all Q_i, where *HSI* values closer to 1 indicate higher organism preference. The *HSI* was assigned for each raster cell depending on its depth and velocity values and the HSC for the life stage of interest. The composite (or combined) habitat suitability index (*cHSI*) for a given fish species and life stage was computed as the geometric mean of depth and velocity *HSIs*. Habitat area (A_{hab}) is defined as the sum of the total wetted area (A_{wet}) whose *cHSI* exceeds a threshold, which was set to 0.5 for this study. Normalized habitat area (A_{hab}/A_{wet}) versus normalized discharge (Q_i/Q_{bf}) curves were generated to remove any potential scaling issues due to differences in channel size. The index of agreement (I_a) between the normalized habitat area curves of the surveyed baseline and any one synthetic terrain indicated how well that synthetic terrain captured habitat conditions across modelled discharges. The I_a was calculated by

$$I_a = 1 - \frac{\sum_{i=1}^{m}(y_i - f_i)^2}{\sum_{i=1}^{m}\left(|f_i - \underline{y}| + |y_i - \underline{y}|\right)^2} \quad (2)$$

where y_i and f_i are the normalized habitat area curves of surveyed and a synthetic terrain, respectively, $\underline{y}$ is the mean of y_i and m is the number of points (i.e. discharge values). An I_a closer to 1 indicates the synthetic terrain parsimoniously replicates baseline ecohydraulic conditions more accurately. Habitat area curve I_a was calculated for each species and life stage, and the best-performing archetype for each combination was indicated by the highest I_a value.

3.7 | Synthesis of test metrics

The overall goal for data analysis was to assess how well synthetic channel scenarios with different variability functions mimic baseline scenarios in terms of hydraulic and ecohydraulic conditions. For hydraulic conditions, we evaluated the KLD value between the joint PDFs of archetypes (four archetypes) and the baseline scenario for each site (three sites) for each flow condition (two flow conditions: baseflow and bankfull). The total number of KLD values is $4 \times 3 \times 2 = 24$. We identified the best-performing archetype (one archetype) whose KLD value is the smallest for each site (three sites) for each flow condition (two flow conditions), and the channel variability function used in the best-performing archetype was identified as a key parameter describing hydraulic responses of a channel. In addition, the KLD value between the marginal PDFs of depth and velocity is reported in Table S2 in supporting information. We tested our hypotheses (1) for baseflow and (2)–(4) for bankfull condition by comparing the identified geomorphic variability function with our expectations. For ecohydraulic conditions, we calculated I_a of flow–habitat curves of archetypes (four archetypes) and the baseline scenario for each site (three sites) and determined the best-performing archetype (one archetype) whose I_a is the largest for each site (three sites). We evaluated our hypothesis (5) by assessing whether the best-performing archetype in ecohydraulic conditions matched with the one resulted from hydraulic conditions.

4 | RESULTS

We present the results of three study sites, SFE 322, 25 and 209, whose identified dominant channel variability functions were thalweg bed undulation, width variation and bed roughness, respectively. Figure S6 shows the representative photos of the field sites, 3D baseline topographies and their channel scenarios with dominant variability functions.

4.1 | Hydraulic performance of synthetic terrains

The best-performing channel scenario producing the smallest KLD with baseline scenario depended on flow conditions. For baseflow condition, the joint PDF of scenario *s2* (thalweg bed undulation) produced the smallest KLD with that of baseline scenario for SFE 322 and 25. On the other hand, in SFE 209, a high-gradient, cobble-boulder and step-pool/cascade channel, scenario *s0* (bed roughness) yielded the best performance in replicating baseline scenario hydraulic conditions. We found that hypothesis (1) was partially corroborated for SFE 322 and 25 and not for SFE 209 although the performance of *s2* was comparable to that of *s0*. Thus, we conclude that the channel variability functions associated with bed topography—thalweg bed undulation or bed roughness—characterize the essential hydraulic responses of a baseline scenario at low flows.

The joint PDFs of depth and velocity from surveyed and synthetic terrains at bankfull flow are shown in Figure 2 for SFE 322, 25 and 209. The joint PDF of baseline scenario hydraulics for site SFE 322 formed two clusters: one with low velocities (<2 m/s) and the other with high velocities (3–6 m/s). Among channel scenarios, only *s2* was able to produce the low-velocity population, which is crucial for fish in all stages. The KLD values for *n0*, *s0*, *s1* and *s2* were 23.68, 19.79, 24.16 and 9.49 for baseflow condition and 9.71, 6.93, 9.26 and 3.40 for bankfull condition. For both flow conditions, scenario *s2* with bed undulations produced the optimal depth and velocity distributions followed by *s0*, implying the thalweg bed elevation explains the major sub-reach-scale hydraulic variabilities. We corroborated hypothesis (2) that s2 with thalweg bed elevation produced the best performance in a high-order mainstem stream with gravel-cobble, high width-to-depth ratio, riffle-pool channel.

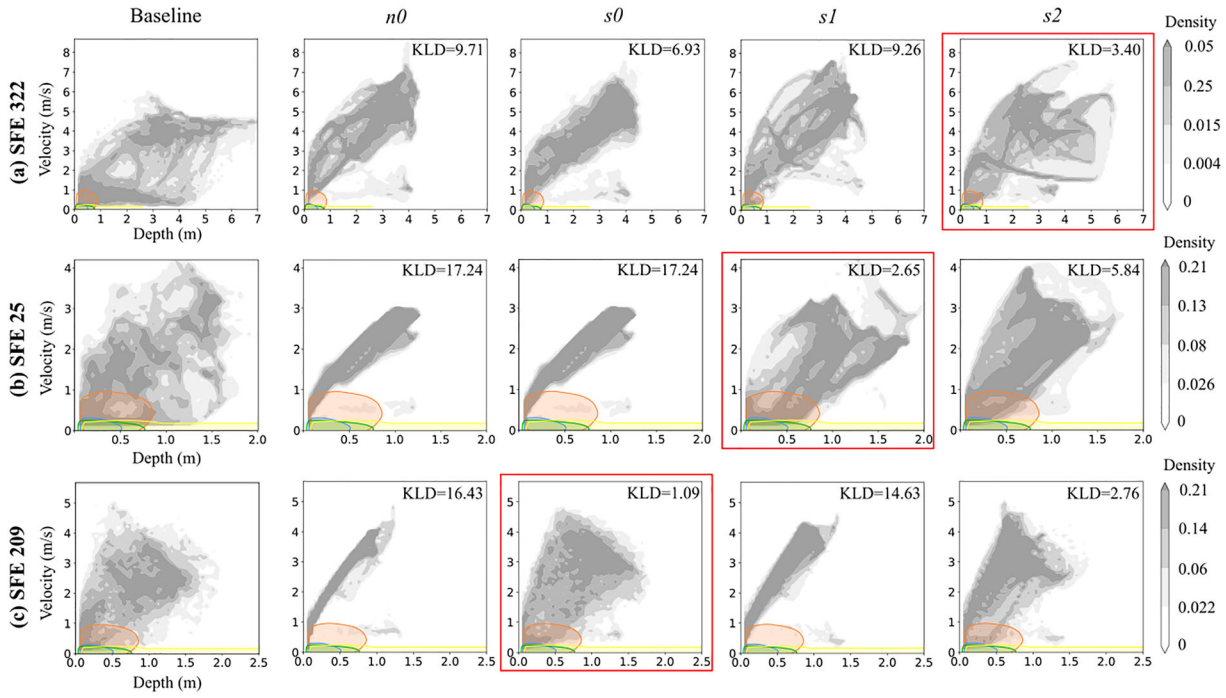

FIGURE 2 Joint probability distribution function (PDF) of hydraulic variables, depth (x-axis) and velocity (y-axis) at bankfull flow with its Kullback–Leibler divergence (KLD) value for (a) SFE 322, (b) SFE 25 and (c) SFE 209. The best-performing scenario that produced the smallest KLD for each site is indicated by a red outline. Contour levels are delineated by 20, 40, 60 and 80 percentiles of the baseline scenario's joint PDF. Overlaid contours illustrate the range of depth and velocity producing high quality habitat (e.g. *cHSI* > 0.5) for fry steelhead (blue), juvenile steelhead (orange), fry coho (green) and juvenile coho (yellow).

The joint PDF of baseline scenario hydraulics for SFE 25 was distributed around the $y = 2x$ line, where x and y indicate depth and velocity, respectively (Figure 2b). Scenario *n0* produced a joint PDF densely distributed around a linear function with a steeper slope, $y = 3x$, failing to yield low-depth and low-velocity populations. For this site, note that *s0* was identical to *n0* because the roughness height was set to 0. The joint PDF of scenario *s1* was mostly populated within the boundary generated from the baseline scenario's case. Although scenario *s2* produced a joint PDF that is similar to the baseline scenario, it generated fewer low velocities and more high velocities. The KLD values for *n0*, *s0*, *s1* and *s2* were 25.10, 25.09, 22.10 and 5.00 for baseflow condition and 17.24, 17.24, 2.65 and 5.84 for bankfull condition. For baseflow, the joint PDF of scenario *s2* with thalweg bed undulation produced the smallest deviation with the baseline scenario. Scenario *s1* with width variability showed the best performance in replicating the depth and velocity distributions of the baseline scenario followed by *s2* for bankfull flow. Thus, we corroborated hypothesis (3) that width variation has the greatest impact in intermediate confined channels characterized by gravel cobble, high-width-to-depth ratio with expansions/contractions.

Site SFE 209 is a 'confined, high-gradient, cobble-boulder, cascade/step-pool' channel whose bed topography is characterized by large sediment including boulders and bedrock. The joint PDF of baseline scenario hydraulics showed a triangular shape while the density was almost uniformly distributed. Scenario *n0* yielded a high-density and narrow distribution centred around a line, $y = 4x$, where x and y are depth and velocity. On the other hand, scenario *s0* generated the joint PDF close to the baseline scenarios' ones. Scenario s1 produced a joint PDF similar to *s0*, but the width was rather widened. Scenario *s2* yielded more diverse range of depth and velocity than s1; however, it did not fully cover the boundary of baseline scenario's distribution. The KLD values for *n0*, *s0*, *s1* and *s2* were 23.32, 1.43, 24.28 and 3.70 for baseflow and 16.43, 1.09, 14.63 and 2.76 for bankfull flow condition. For both baseflow and bankfull conditions, *s0* with bed roughness produced the closest hydraulic responses to baseline scenario followed by *s2*, which validates hypothesis (4). Large boulders were densely placed, and these features characterized the overall channel topography controlling hydraulic responses. This implies that the Perlin bed roughness function can represent the channel topography where there are a significant number of large substrate features on the streambed without having to use RB's object-oriented boulder placement capability.

The average values of KLDs of *n0*, *s0*, *s1* and *s2* were 24.03, 15.44, 23.51 and 6.06 for baseflow and 14.46, 8.42, 8.85 and 4.00 for bankfull condition, respectively (Table 4). Overall, scenario *s2* yielded the best performance for both baseflow and bankfull conditions. The joint PDF of *s2* is widely spread compared to other scenarios producing a range of depths and velocities.

TABLE 4 A summary table of hydraulic and ecohydraulic test metrics and their average values for each channel scenario. The scenario with smallest KLD or largest I_a is highlighted in grey.

Test variables	Test metric, flow condition	Site ID	*n0*	*s0*	*s1*	*s2*
Hydraulics	KLDs of joint PDFs, baseflow	SFE 322	23.68	19.79	24.16	9.49
		SFE 25	25.10	25.10	22.10	5.00
		SFE 209	23.32	1.43	24.28	3.70
		Average	24.03	15.44	23.51	6.06
	KLDs of joint PDFs, bankfull	SFE 322	9.71	6.93	9.26	3.40
		SFE 25	17.24	17.24	2.65	5.84
		SFE 209	16.43	1.09	14.63	2.76
		Average	14.46	8.42	8.85	4.00
Ecohydraulics	I_a of habitat curves, all flow conditions	SFE 322	0.51	0.66	0.50	0.91
		SFE 25	0.59	0.59	0.79	0.76
		SFE 209	0.55	0.96	0.55	0.90
		Average	0.55	0.74	0.61	0.86

4.2 | Ecological performance of synthetic terrains

In general, channel scenarios produced smaller habitat areas compared to their baseline scenario. In addition, scenario *s2* with thalweg bed undulation was the best scenario in replicating ecological response of baseline scenario followed by *s0* with bed roughness. The average I_a values for fry and juvenile steelhead trout were 0.69 and 0.95 and for fry and juvenile coho salmon were 0.59 and 0.67, respectively. The average I_a values for each synthetic channel scenario were 0.62, 0.75, 0.66 and 0.87 for *n0*, *s0*, *s1* and *s2*.

For site SFE 322, the average I_a values of the habitat curves of baseline and channel scenarios *n0*, *s0*, *s1* and *s2* were 0.51, 0.66, 0.50 and 0.91. Only *s2* was able to precisely reproduce the suitable habitat area of the baseline scenario across a range of flow condition. At low discharges (e.g. $Q_i/Q_{bf} < 0.2$), only *s2* was able to produce as much habitat area as the baseline scenario for fry steelhead and fry/juvenile coho salmon (Figure 3a1, a3, a4). At bankfull, the predicted normalized habitat area of all synthetic terrains was less than that of baseline scenario. This is because the synthetic terrains failed to produce small depths and low velocities, which are critical habitat conditions for these species life stages (Figure 3a1). For juvenile coho salmon, all the synthetic channel scenarios were able to produce habitat area curves similar to the baseline scenario.

For SFE 25, the average I_a values between the habitat curves of baseline and channel scenarios were 0.59, 0.59, 0.79 and 0.76 for *n0*, *s0*, *s1* and *s2*. While both scenarios *s1* and *s2* produced relatively high agreement values, *s1* captured the increasing pattern of habitat curve better than *s2* for fry steelhead and fry, juvenile coho (Figure 3b1, b3, b4). For juvenile coho, all channel scenarios generated comparable habitat curves to the baseline scenario and their I_a values were 0.97, 0.97, 0.98 and 0.97 for *n0*, *s0*, *s1* and *s2*.

For SFE 209, the habitat curve of *s0* showed the best match with the baseline scenario for all species and life stages. The average I_a values between the habitat curves of baseline and channel scenarios were 0.55, 0.96, 0.55 and 0.90 for *n0*, *s0*, *s1* and *s2*. For fry steelhead and fry, juvenile coho salmon, only *s0* and *s2* were able to mimic the baseline scenarios' habitat area curve (Figure 3c1, c3, c4). This is because *n0* and *s1* did not generate much small-depth and low-velocity populations, which were critical for fry/juvenile steelhead and fry coho salmon. For juvenile coho salmon, all habitat curves from synthetic terrains resulted in great match with the baseline scenario, yielding high agreement values.

In general, the optimal scenario that best replicated the hydraulic responses of each baseline scenario (e.g. joint PDF of depth and velocity at bankfull) also produced the best matching ecological responses (e.g. habitat curve), which corroborated hypothesis (5). Furthermore, the average I_a values of *n0*, *s0*, *s1* and *s2* were 0.55, 0.74, 0.61, and 0.86. Overall, scenario *s2* captured the habitat curve pattern better than others as it did in hydraulic responses.

5 | DISCUSSION

This study examined which sub-reach channel variability functions among bankfull width variability, thalweg bed elevation variability and bed roughness have the largest effect on the hydraulic and ecohydraulic conditions exhibited by three typical mountain channel reaches and how that varies with flow conditions. We found that (1) thalweg bed elevation had the largest influence in the high-order mainstem stream channel with riffle-pool sequences at both baseflow and bankfull conditions, and in the intermediate confined uniform channel for baseflow condition (hypothesis 1 and 2), (2) width variation had the largest influence in an intermediate confined uniform channel characterized by expansions/contractions for bankfull condition (hypothesis 3) and (3) bed roughness was crucial for replicating hydraulics in the confined, high-gradient, cobble-boulder, step-pool/cascade channel (hypothesis 4). Additionally, (4) the synthetic channel scenario that produced the optimal hydraulic conditions mostly produced the best fit ecohydraulic conditions compared to baseline scenario (hypothesis 5).

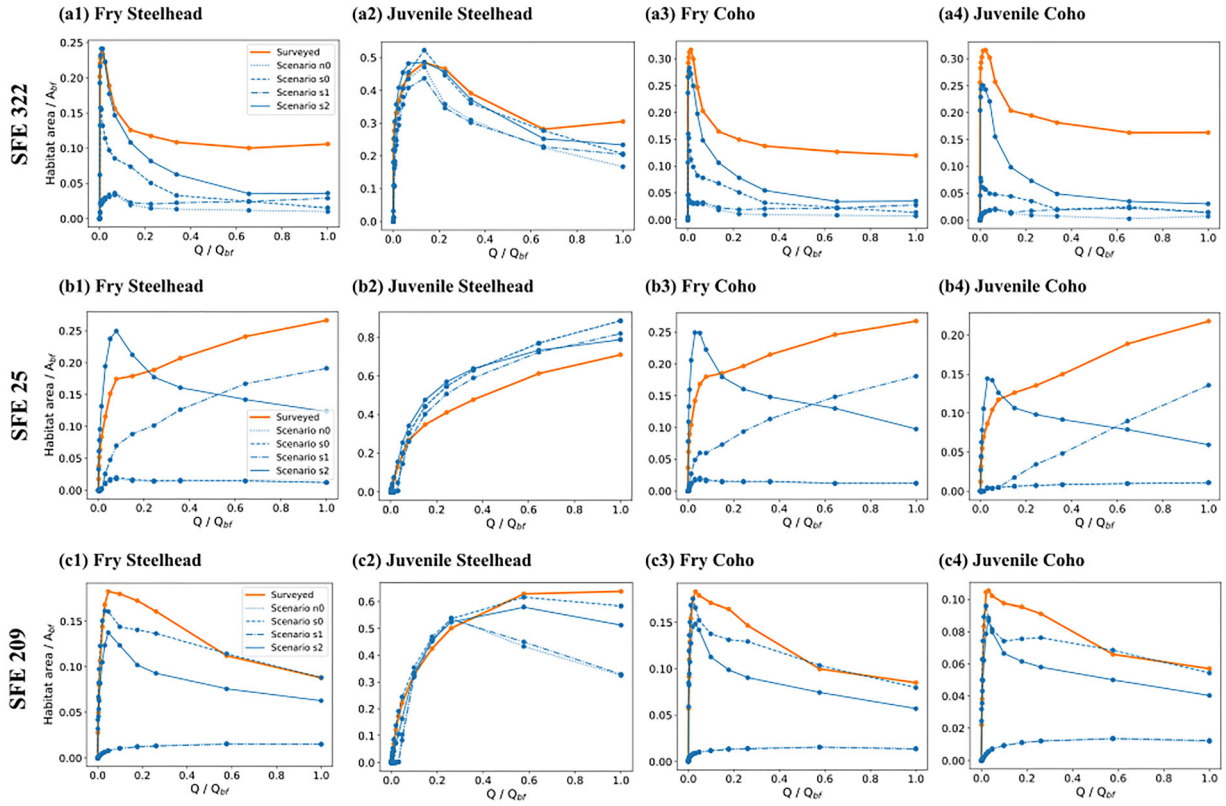

FIGURE 3 Normalized habitat area curves generated using the baseline scenario (orange bold line) and synthetic channel terrain scenarios (blue dotted, *n0*; blue dashed, *s0*; blue dash-dotted, *s1*; and blue solid line, *s2*) for three study reaches, (a) SFE 322, (b) SFE 25 and (c) SFE 209, and fry/juvenile steelhead and coho salmon.

Our study provides a framework to create a synthetic river channel in River Builder through reverse-engineering and proposed performance metrics to assess the resemblance of different terrains based on their hydraulic and ecohydraulic conditions across discharges, which may facilitate the process of designing and managing rivers. One can develop a site-specific synthetic channel, which serves as an approximate landform model using the best available information among width variation, thalweg bed undulation and bed roughness height to evaluate its potential ecohydraulic responses. Other hydro-ecosystem function metrics such as geomorphic stability (Doyle et al., 2000), hydrogeomorphic diversity (Gostner et al., 2013), salmonid bed preparation and occupation (Escobar-Arias & Pasternack, 2010), redd dewatering risk (Becker & Neitzel, 1985) and eco-reliability and sustainability (Lane et al., 2020) can be further added to this framework as needed to evaluate the performance of other ecosystem functions.

Results from this study can help reduce field data collection efforts by prioritizing the channel variability features that need to be surveyed based on a reach's pre-defined channel type (e.g. Guillon et al., 2020). For example, for channel reaches without significant contraction/expansion in widths or densely placed boulders, rather than requiring a total station survey or other resource intensive approach to generate feature-based channel terrain, one may only need thalweg elevation measurements and reach-average dimensions to generate a synthetic terrain capable of reproducing suitability maps of sufficient accuracy for some applications. For regions with potential drought risk, thalweg bed undulation should be included in a site survey as they control the ecohydraulic responses of a channel at low flows. Furthermore, this framework can be used for river restoration design by isolating and iteratively altering certain channel features to find the optimal channel design scenario appropriate for the region of interest.

Future research could examine the effect of the surveyed data quality (e.g. accuracy, resolution, minimum point density) on the performance of the synthetic channel in replicating the surveyed terrain's ecohydraulic responses to determine the minimum accuracy/resolution required for a field survey to reduce surveying efforts. This would free up resources to evaluate more channel reaches across a region to facilitate larger scale habitat suitability or instream flow analysis, a critical goal of natural resource managers in SFER catchment, California and other arid regions worldwide.

As our approach is developed based on specific experimental settings and assumptions, one should be mindful of the following constraints and limitations when applying it to other settings. First, there are many other important sub-reach-scale geomorphic variability functions, geomorphic units and settings that are not considered in this study. For example, we did not evaluate point/braid bars (Ock et al., 2015), floodplains (Richards et al., 2002), manmade structures (Able et al., 1999; Moschella et al., 2005) or the effects of riparian

vegetation (Corenblit et al., 2007). Second, we evaluated hydraulic conditions based on the joint PDF of depth and velocity, and ecological conditions based on the habitat area curve. Not only the population of the depths and velocities but also their spatial pattern is crucial in determining the habitat patch network, which affects the organism behaviour (Isaak et al., 2007; Pasternack & Tu, 2016).

Importantly, this framework can now be readily applied to evaluate other sub-reach-scale variability functions based on distinct statistical properties of geomorphic attributes such as geomorphic covariance structures (Brown & Pasternack, 2014; Pasternack et al., 2021), coefficient of variance of width and depth (Guillon et al., 2020; Lane et al., 2017) or fractal dimension (Guillon et al., 2020) for different channel type. This would help us to estimate hydraulic and ecological responses of a watershed with limited topographic information by enabling one to synthesize a generic channel corridor without any field survey data.

6 | CONCLUSION

We examined which sub-reach channel variability functions among longitudinal bankfull width variability, thalweg bed elevation variability and bed roughness have the largest effect on the hydraulic and ecohydraulic conditions exhibited by three typical mountain channel reaches and how that varies with flow conditions. We developed four parsimonious synthetic channel archetypes (Scenarios *n0*, *s0*, *s1* and *s2*) comprising different channel variability functions to mimic each of three channel reaches surveys spanning various geomorphic channel types. The best synthetic channel scenario was identified and the associated variability function in terms of their ability to reproduce survey-based hydraulic and ecohydraulic conditions.

We found that (1) thalweg bed elevation had the largest influence in the high-order mainstem stream with riffle-pool sequences at both baseflow and bankfull conditions, and the intermediate confined uniform channel for baseflow condition, (2) width variation played a key role in intermediate confined uniform channels characterized by expansions/contractions for bankfull condition, and (3) bed roughness was crucial for replicating the confined, high-gradient, cobble-boulder, step-pool/cascade channel. Additionally, (4) the synthetic channel scenario that produced the optimal hydraulic conditions mostly produced the best fit ecohydraulic conditions compared to baseline scenario.

This study provides a framework to create a reverse-engineered river corridor and proposed performance metrics to assess the resemblance of different terrains based on their hydraulic and ecohydraulic conditions across discharges, which may facilitate the process of designing and managing rivers. Furthermore, this framework can now be readily applied to evaluate other sub-reach-scale variability functions based on distinct statistical properties of geomorphic attributes. This would help to estimate hydraulic and ecological responses of a watershed with limited topographic information by enabling generic river corridors to be synthesized without any field survey data.

ACKNOWLEDGEMENTS

This research was supported by the California State Water Resources Control Board under grant number 16-062-300. The authors also acknowledge the USDA National Institute of Food and Agriculture, Hatch project numbers CA-D-LAW-7034-H, and the Utah Water Research Laboratory, Utah State University. We thank Dr Samuel Sandoval for his contributions to the project conceptualization and Alison O'Dowd, Mason London, and Emily Cooper for data collection. We thank Muwei Zheng and Xavier Nogueira for their contributions to development of River Builder and associated toolsets.

DATA AVAILABILITY STATEMENT

The data that support the findings of this study are available on request from the corresponding author. The data are not publicly available due to privacy or ethical restrictions.

ORCID

Anzy Lee https://orcid.org/0000-0003-0487-1287
Belize Lane https://orcid.org/0000-0003-2331-7038
Gregory B. Pasternack https://orcid.org/0000-0002-1977-4175

REFERENCES

Able, K. W., Manderson, J. P., & Studholme, A. L. (1999). Habitat quality for shallow water fishes in an urban estuary: The effects of man-made structures on growth. *Marine Ecology Progress Series*, *187*, 227–235. https://doi.org/10.3354/meps187227

Anim, D. O., Fletcher, T. D., Vietz, G. J., Burns, M. J., & Pasternack, G. B. (2019). How alternative urban stream channel designs influence ecohydraulic conditions. *Journal of Environmental Management*, *247*, 242–252. https://doi.org/10.1016/j.jenvman.2019.06.095

Asarian, J. E. (2015). Long-term streamflow and precipitation trends in the Eel river basin. Prepared by Riverbend Sciences for Friends of the Eel River, Arcata, CA. 30p. + appendices.

Becker, C. D., & Neitzel, D. A. (1985). Assessment of intergravel conditions influencing egg and alevin survival during salmonid redd dewatering. *Environmental Biology of Fishes*, *12*(1), 33–46. https://doi.org/10.1007/BF00007708

Bouwes, N., Moberg, J., Weber, N., Bouwes, B., Bennett, S., Beasley, C., Jordan, C.E., Nelle, P., Polino, M., Rentmeester, S., Semmens, B., Volk, C., Ward, M.B., and White, J. (2011). Scientific protocol for salmonid habitat surveys within the Columbia Habitat Monitoring Program. Project #2011-006. The Integrated Status and Effectiveness Monitoring Program.

Brown, R. A., & Pasternack, G. B. (2009). Comparison of methods for analysing salmon habitat rehabilitation designs for regulated rivers. *River Research and Applications*, *25*(6), 745–772. https://doi.org/10.1002/rra.1189

Brown, R. A., & Pasternack, G. B. (2014). Hydrologic and topographic variability modulate channel change in mountain rivers. *Journal of Hydrology*, *510*, 551–564. https://doi.org/10.1016/j.jhydrol.2013.12.048

Brown, R. A., & Pasternack, G. B. (2017). Analyzing bed and width oscillations in a self-maintained gravel-cobble bedded river using geomorphic covariance structures. *Earth Surface Dynamics*, *4*(1), 1–48. https://doi.org/10.5194/esurf-2015-49

Brown, R. A., Pasternack, G. B., & Lin, T. (2016). The topographic design of river channels for form-process linkages. *Environmental Management*, *57*, 929–942. https://doi.org/10.1007/s00267-015-0648-0

Bureau of Land Management (BLM). (1996). South Fork Eel River watershed analysis. Bureau of Land Management: Six Rivers National Forest

and US Fish and Wildlife Service: Coastal California Fish and Wildlife Office. Available online at: https://archive.org/stream/southforkeelrive7894full#page/n0/mode/2up

Bureau of Land Management (BLM). (2001). Interagency vegetation mapping project, western cascades (version 2.0) and western lowlands (version 1.0) spatial data, 1996. Available: http://www.or.blm.gov/gis/projects/vegetation. (August 2003)

Byrne, C. F., Guillon, H., Lane, B. A., Pasternack G. B., & Sandoval-Solis, S. (2020). Coastal California regional geomorphic classification. Final report. Submitted to the California State Water Resources Control Board. Davis, California. February 2019.

California Department of Fish and Wildlife. (2014) South Fork Eel River watershed assessment. Coastal Watershed Planning and Assessment Program. California Department of Fish and Wildlife.

California Department of Fish and Wildlife. (2020). Habitat suitability criteria for juvenile salmonids in the South Fork Eel River watershed, Mendocino and Humboldt counties. Stream evaluation report, 2020–2001.

Cao, Z., Carling, P., & Oakey, R. (2003). Flow reversal over a natural pool-riffle sequence: A computational study. *Earth Surface Processes and Landforms*, *28*, 689–705. https://doi.org/10.1002/esp.466

Cardenas, M. B. (2009). A model for lateral hyporheic flow based on valley slope and channel sinuosity. *Water Resources Research*, *45*(1), W01501. https://doi.org/10.1029/2008WR007442

Coastal Watershed Planning & Assessment Program (CWPAP). (2014). The South Fork Eel River assessment report. Available online at: http://coastalwatersheds.ca.gov/tabid/739/Default.aspx

Corenblit, D., Tabacchi, E., Steiger, J., & Gurnell, A. M. (2007). Reciprocal interactions and adjustments between fluvial landforms and vegetation dynamics in river corridors: A review of complementary approaches. *Earth-Science Reviews*, *84*(1–2), 56–86. https://doi.org/10.1016/j.earscirev.2007.05.004

Doyle, M. W., Harbor, J. M., Rich, C. F., & Spacie, A. (2000). Examining the effects of urbanization on streams using indicators of geomorphic stability. *Physical Geography*, *21*(2), 155–181. https://doi.org/10.1080/02723646.2000.10642704

Eel River Action Plan. (2016) A compilation of information and recommended actions. The Eel River forum. Available online at: https://eelriver.org/wp-content/uploads/2020/03/Eel-River-Action-Plan-2016.pdf

Escobar-Arias, M. I., & Pasternack, G. B. (2010). A hydrogeomorphic dynamics approach to assess in-stream ecological functionality using the functional flows model, part 1-model characteristics. *River Research and Applications*, *26*, 1103–1128. https://doi.org/10.1002/rra.1316

Escobar-Arias, M. I., & Pasternack, G. B. (2011). Differences in river ecological functions due to rapid channel alteration processes in two California rivers using the functional flows model, part 2—Model applications. *River Research and Applications*, *27*(1), 1–22. https://doi.org/10.1002/rra.1335

Fenicia, F., Savenije, H. H. G., Matgen, P., & Pfister, L. (2007). A comparison of alternative multiobjective calibration strategies for hydrological modeling. *Water Resources Research*, *43*, W03434. https://doi.org/10.1029/2006WR005098

Freedman, D., & Diaconis, P. (1981). On the histogram as a density estimator: L2 theory. *Probability Theory and Related Fields*, *57*(4), 453–476. https://doi.org/10.1007/BF01025868

Freiknecht, J., & Effelsberg, W. (2017). A survey on the procedural generation of virtual worlds. *Multimodal Technologies and Interaction.*, *1*(4), 27. https://doi.org/10.3390/mti1040027

French, J. R., & Clifford, N. J. (2000). Hydrodynamic modeling as a basis for explaining estuarine environmental dynamics: Some computational and methodological issues. *Hydrological Processes*, *14*, 2089–2108. https://doi.org/10.1002/1099-1085(20000815/30)14:11/12<2089::AID-HYP56>3.0.CO;2-L

Gostner, W., Alp, M., Schleiss, A. J., & Robinson, C. T. (2013). The hydro-morphological index of diversity: A tool for describing habitat heterogeneity in river engineering projects. *Hydrobiologia*, *712*, 43–60. https://doi.org/10.1007/s10750-012-1288-5

Guillon, H., Byrne, C. F., Lane, B. A., Pasternack G. B., & Sandoval-Solis, S. (2019). South Fork Eel River basin geomorphic classification. Final report. Submitted to the California State Water Resources Control Board. Davis, California. February 2019.

Guillon, H., Byrne, C. F., Lane, B. A., Sandoval Solis, S., & Pasternack, G. B. (2020). Machine learning predicts reach-scale channel types from coarse-scale geospatial data in a large river basin. *Water Resources Research*, *56*, e2019WR026691. https://doi.org/10.1029/2019WR026691

Hack, J. T., & Goodlett, J. C. (1960). Geomorphology and forest ecology of a mountain region in the central Appalachians (No. 347). United States Government Printing Office.

Instream Flow Study Plan. (2016). Habitat and instream flow evaluation for anadromous salmonids in the South Fork Eel River and tributaries, Humboldt and Mendocino counties. California Department of Fish and Wildlife. Available online at: https://nrm.dfg.ca.gov/FileHandler.ashx?DocumentID=118161&inline

Isaak, D. J., Thurow, R. F., Rieman, B. E., & Dunham, J. B. (2007). Chinook salmon use of spawning patches: Relative roles of habitat quality, size and connectivity. *Ecological Applications*, *17*(2), 352–364. https://doi.org/10.1890/05-1949

Jackson, J. R., Pasternack, G. B., & Wheaton, J. M. (2015). Virtual manipulation of topography to test potential pool–riffle maintenance mechanisms. *Geomorphology*, *228*, 617–627. https://doi.org/10.1016/j.geomorph.2014.10.016

Kullback, S., & Leibler, R. A. (1951). On information and sufficiency. *Annals of Mathematical Statistics*, *22*(1), 79–86. https://doi.org/10.1214/aoms/1177729694

Lane, B., Ortiz-Partida, J. P., & Sandoval-Solis, S. (2020). Extending water resources performance metrics to river ecosystems. *Ecological Indicators*, *114*, 106336. https://doi.org/10.1016/j.ecolind.2020.106336

Lane, B., Pasternack, G. B., & Sandoval-Solis, S. (2018). Integrated analysis of flow, form, and function for river management and design testing. *Ecohydrology*, *11*, e1969. https://doi.org/10.1002/eco.1969

Lane, B. A., Pasternack, G. B., Dahlke, H. E., & Sandoval-Solis, S. (2017). The role of topographic variability in river channel classification. *Progress in Physical Geography*, *41*(5), 570–600. https://doi.org/10.1177/0309133317718133

Lee, A., Aubeneau, A. F., & Cardenas, M. B. (2020). The sensitivity of hyporheic exchange to fractal properties of riverbeds. *Water Resources Research*, *56*, e2019WR026560. https://doi.org/10.1029/2019WR026560

Moschella, P. S., Abbiati, M., Åberg, P., Airoldi, L., Anderson, J. M., Bacchiocchi, F., … Hawkins, S. J. (2005). Low-crested coastal defence structures as artificial habitats for marine life: Using ecological criteria in design. *Coastal Engineering*, *52*(10–11), 1053–1071. https://doi.org/10.1016/j.coastaleng.2005.09.014

Ock, G., Gaeuman, D., McSloy, J., & Kondolf, G. M. (2015). Ecological functions of restored gravel bars, the Trinity River, California. *Ecological Engineering*, *83*, 49–60. https://doi.org/10.1016/j.ecoleng.2015.06.005

Pasternack, G. B., Bounrisavong, M. K., & Parikh, K. K. (2008). Backwater control on riffle–pool hydraulics, fish habitat quality, and sediment transport regime in gravel-bed rivers. *Journal of Hydrology*, *357*(1–2), 125–139. https://doi.org/10.1016/j.jhydrol.2008.05.014

Pasternack, G. B., Gore, J. L., & Wiener, J. S. (2021). Geomorphic covariance structure of a confined mountain river reveals landform organization stage threshold. *Earth Surface Processes and Landforms*, *46*(13), 2582–2606. https://doi.org/10.1002/esp.5195

Pasternack, G. B., & Tu, D. (2016) Chinook salmon spawning site selection is influenced by size of microhabitat patch. 11th International Symposium on Ecohydarulics. Melbourne, Australia.

Pasternack, G. B., and Zhang, M. (2021) River builder user's manual for version 1.2.0. University of California, Davis, CA.

Petrucci, G., & Bonhomme, C. (2014). The dilemma of spatial representation for urban hydrology semi-distributed modelling: Trade-offs among complexity, calibration and geographical data. *Journal of Hydrology*, *517*, 997–1007. https://doi.org/10.1016/j.jhydrol.2014.06.019

Richards, K., Brasington, J., & Hughes, F. (2002). Geomorphic dynamics of floodplains: Ecological implications and a potential modelling strategy. *Freshwater Biology*, *47*, 559–579. https://doi.org/10.1046/j.1365-2427.2002.00920.x

Rosgen, D. L. (1994). A classification of natural rivers. *Catena*, *22*, 169–199. https://doi.org/10.1016/0341-8162(94)90001-9

Schwindt, S., Larrieu, K., Pasternack, G. B., & Rabone, G. (2020). River architect. https://doi.org/10.1016/j.softx.2020.100438

Sear, D. A., & Newson, M. D. (2004). The hydraulic impact and performance of a lowland rehabilitation scheme based on pool–riffle installation: The river Waveney, Scole, Suffolk, UK. *River Research and Applications*, *20*(7), 847–863. https://doi.org/10.1002/rra.791

Smith, R. D., Ammann, A., Bartoldus, C., & Brinson, M. M. (1995). An approach for assessing wetland functions using hydrogeomorphic classification, reference wetlands, and functional indices. ARMY ENGINEER WATERWAYS EXPERIMENT STATION VICKSBURG MS.

Syme, W. (2001) TUFLOW-Two & One dimensional unsteady flow software for rivers, estuaries and coastal waters. In: Paper Presented at the IEAust Water Panel Seminar and Workshop on 2d Flood Modelling, (Sydney).

Thomson, J. R., Taylor, M. P., Fryirs, K. A., & Brierley, G. J. (2001). A geomorphological framework for river characterization and habitat assessment. *Aquatic Conservation: Marine and Freshwater Ecosystems*, *11*, 373–389. https://doi.org/10.1002/aqc.467

Trauth, N., Schmidt, C., Maier, U., Vieweg, M., & Fleckenstein, J. H. (2013). Coupled 3-D stream flow and hyporheic flow model under varying stream and ambient groundwater flow conditions in a pool-riffle system. *Water Resources Research*, *49*(9), 5834–5850. https://doi.org/10.1002/wrcr.20442

Vannote, R. L., & Sweeney, B. W. (1980). Geographic analysis of thermal equilibria: A conceptual model for evaluating the effect of natural and modified thermal regimes on aquatic insect communities. *The American Naturalist*, *115*(5), 667–695. https://doi.org/10.1086/283591

Wagener, T., Lees, M. J., & Wheater, H. S. (2001). A toolkit for the development and application of parsimonious hydrological models. *Mathematical Models of Small Watershed Hydrology*, *1*, 87–136.

Wohl, E. E., Thompson, D. M., & Miller, A. J. (1999). Canyons with undulating walls. *Geological Society of America Bulletin*, *111*, 949–959. https://doi.org/10.1130/0016-7606(1999)111<0949:CWUW>2.3.CO;2

Yang, X., Magnusson, J., Huang, S., Beldring, S., & Xu, C. (2020). Dependence of regionalization methods on the complexity of hydrological models in multiple climatic regions. *Journal of Hydrology*, *582*, 124357. https://doi.org/10.1016/j.jhydrol.2019.124357

Yoshiyama, R. M., & Moyle, P. B. (2010). Historical review of Eel River anadromous salmonids, with emphasis on Chinook salmon, coho salmon and steelhead. UC Davis, Center for watershed sciences. https://eelriver.org/wp-content/uploads/2017/07/Yoshiyama-Moyle_Historical-Reivew-of-Eel-River-Anadromous-Salmonids-Final-Report-2010.pdf

SUPPORTING INFORMATION

Additional supporting information can be found online in the Supporting Information section at the end of this article.

How to cite this article: Lee, A., Lane, B., & Pasternack, G. B. (2023). Identifying key channel variability functions controlling ecohydraulic conditions using synthetic channel archetypes. *Ecohydrology*, e2533. https://doi.org/10.1002/eco.2533

Supporting Information for

Identifying key channel variability functions controlling ecohydraulic conditions using synthetic channel archetypes

Anzy Lee[1], Belize A. Lane[1], Gregory B. Pasternack[2]

[1]Civil and Environmental Engineering, Utah State University, Logan, UT, USA

[2]Department of Land, Air & Water Resources, University of California Davis, Davis, CA, USA

Introduction

This supporting document provides additional information, tables and figures.

Contents of this file

Tables

Figures

Reverse engineering geometric functions from baseline scenarios

The following procedure "reverse engineers" a parsimonious geometric function from a spatial series of any longitudinal feature of a river corridor. On the basis of this workflow (Figure S1), we briefly demonstrate how the geometric and hydraulic variables, Table 3 column [B], were extracted from each baseline scenario's 2D hydrodynamic simulation results to inform synthetic channel design using site SFE 322. The simulation condition for 2D hydrodynamic modeling is described in the following section, 3.4. More details on the RB software and methods are available in the user's manual.

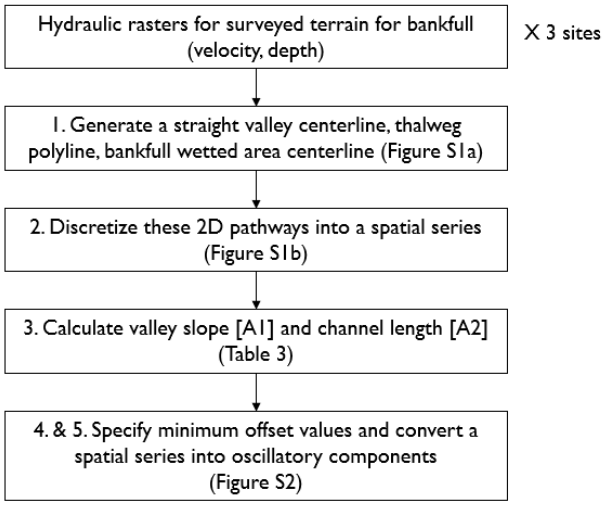

Figure S1. Workflow of reverse engineering geometric functions from baseline scenarios

First, 2D pathways were generated from the baseline scenario of a real terrain and its bankfull discharge (Q_{bf}) 2D model simulation. For this study six types of 2D pathways were created (Figure S2a) including: an XY (i.e., longitudinal-lateral, planform plane) straight valley centerline, an XY sinuous thalweg polyline, an XY sinuous bankfull wetted area centerline, an XZ (i.e., longitudinal elevation plane) thalweg bed undulation polyline, XZ water surface elevation polyline and numerous YZ (i.e., lateral elevation plane) river cross-sections. The valley centerline simply connected the upstream and downstream endpoints of the channel centerline. The XY thalweg followed the path of steepest descent in the bed elevation raster. The XY channel centerline bisected the bankfull wetted area polygon.

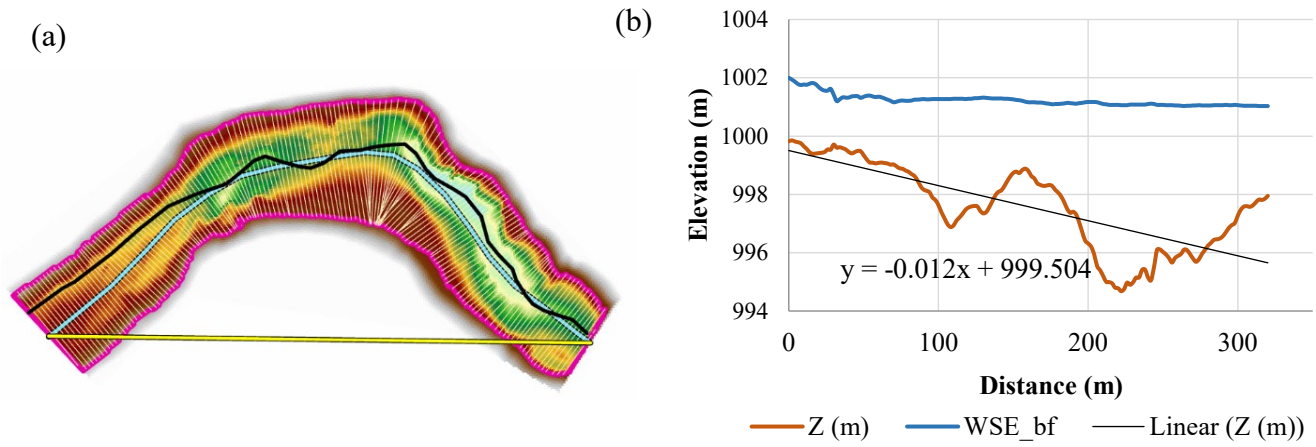

Figure S2. (a) A surveyed topography of SFE 322 with a straight line (yellow line), thalweg (black line), centerline of the channel (sky-blue line) and transect lines perpendicular to the centerline (thin yellow lines) (b) Water surface profile (blue), bed elevation (brown) at the thalweg and its regression line (black)

To provide maximum flexibility, RB procedurally generates each inner-channel bank function (left and right) independently with as many user-defined planform functions as desired for each bank. If desired, the two banks can be assigned the same function to have them patterned the same way with a symmetrical outcome. A symmetrical approach was used in this study, such that each bank function got half the amplitude of total channel width.

Second, each of these 2D pathways was discretized into a spatial series. The interval of points spacing should be selected on the basis of an understanding of topographic and hydraulic model resolution. For this study, point series for a given baseline scenario were stationed in 1-m or 2-m intervals depending on whether reach bankfull wetted area was $<$ or $\geq$ 5000 m^2, respectively. Planform series were represented with $\{x, y\}$ coordinates, while elevation series (bed, water depth, and water surface) were represented with $\{x, j\}$ coordinates, where j could be bed elevation, water depth, or water surface elevation. For the bankfull width series, centerline-orthogonal (i.e., cross-sectional) lines were generated at these stations with an initial length well exceeding maximum bankfull width. Transect lines were then clipped with the bankfull wetted area polygon to obtain their correct lengths (thin yellow lines in Figure S2a) and each length value (i.e., width) was assigned to both the transect line and the centerline station point. At this point, all spatial series were available for use either in ArcGIS or extracted to text files for use in Python algorithms.

Third, two reach-average metrics were calculated from spatial series to set up the spatial domain of the archetype. Valley slope [A1] was calculated as the slope of the linear regression of the thalweg bed elevation profile (Figure S2b). Channel length [A2] was calculated as the length of the straight line connecting the starting and ending points of the channel (thick yellow line in Figure S2a).

Fourth, no matter what type of geometric function is selected to represent a spatial series, there will always need to be a minimum offset distance chosen to ensure that a 2D function does not cross over with any other adjacent 2D function. For example, one would not want the left bank and the channel centerline to cross each other. Given a sufficiently complex geometric function for any planform contour and applied to follow along any arbitrarily sinuous centerline (possibly also nested within a sinuous valley centerline), one cannot analytically reason out whether a cross-over is at risk. Specifying a minimum offset distance between a planform geometric function and the next closest one (closer to the channel centerline) solves the problem.

For this study, minimum offset distances were needed for each bank-top planform function (i.e., left and right lateral offsets from the centerline) as well as for the thalweg bed elevation (to ensure the bed did not go higher than bank tops). The minimum value of the spatial series of bankfull width was divided by two and used as an inner channel lateral offset minimum for each bank (thus yielding a width symmetrical about the centerline) [B4]. Likewise, the minimum value of thalweg water depth was used as the inner channel depth minimum [B5].

Having established minimum offset values, the fifth step involved selecting a geometric function to represent each 2D spatial series among the various types previously listed. Because all the channels in this study were in confined mountain canyons or narrow valleys, sinuosity was not an important feature to be concerned with. As a result, the XY wetted area centerline function that generates river sinuosity was described simply as a single half-sinusoidal wave whose amplitude is the maximum distance between the straight line and centerline, frequency is 1/2, and phase is 0. All other XY and XZ spatial series fit with functions in this study involved a summation of sinusoidal functions of different frequencies, because that was the easiest function to use to reverse engineer spatial series. Future reverse engineering additions could include use of wavelets, empirical orthogonal functions, or a combination of multiple methods in a suitable prioritization order (Kalbermatten et al., 2012; Kuriyama and Yanagishima, 2016).

A Fourier analysis was performed to decompose the original geometric spatial series from the baseline scenario into oscillatory components. There is no limit to how many sinusoidal frequency components one can use to try to represent a spatial series, so a criterion was chosen to establish a threshold of parsimonious representation. Specifically, we decided that the goal was to obtain a representation for which the coefficient of determination (r^2) between the original series and reconstructed series was ≥ 0.9. To achieve this, the lowest frequency component was used to create a spatial series and this was tested against the real spatial series to obtain the r^2 value. If this was < 0.9, then the next lowest frequency component was added to the archetype and the resulting combination tested against the criterion. Incrementally higher frequency components were added one-at-a-time until the criterion was met.

Figure S3 illustrates the outcome by comparing the original (blue line) and reconstructed bankfull width (red dashed line) series for site SFE 322. The black line is a zero-averaged width function, which is a required preprocessing step for Fourier analysis. The red dashed line is the reconstructed signal made using the seven lowest-frequency harmonic components. The amplitude, phase, and wavelength of these oscillatory components is stored in a separate txt file, along with the minimum lateral offset for the reconstructed signal.

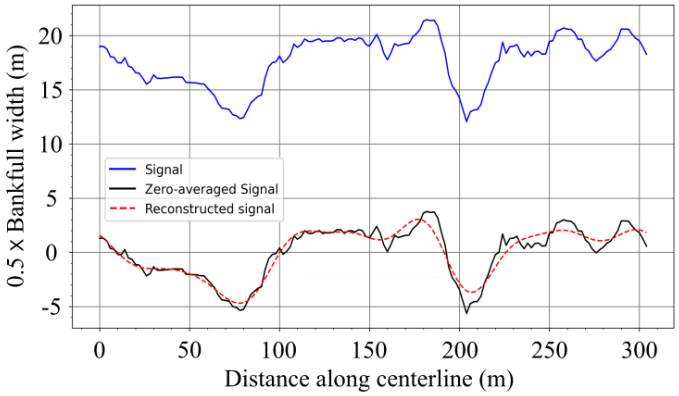

Figure S3. Harmonic decomposition and reconstruction of a bankfull width: the blue line represents the original bankfull width variation, the black line is the zero-averaged bankfull width and the red dotted line is reconstructed zero-averaged bankfull width function

Table S1. Summary table for cross-sectional shape of the inner channel, Perlin bed roughness height, and 2D hydrodynamic modeling parameters. AU and SU refer to asymmetrical U-shape and symmetrical U-shape, respectively.

Site ID	Cross-sectional shape	Perlin bed roughness height (m)	Bankfull Discharge (cms)	Cell size (m)	Slope	Manning's n (Surveyed)
SFE 322	AU	0.5	110.48	1	0.0559	0.043
SFE 25	SU	0	44.296	1	0.0069	0.037
SFE 209	SU	1	13.96	0.3	0.094	0.079

Figure S4. Sensitivity analysis on grid size when converting TIN surface to raster topography

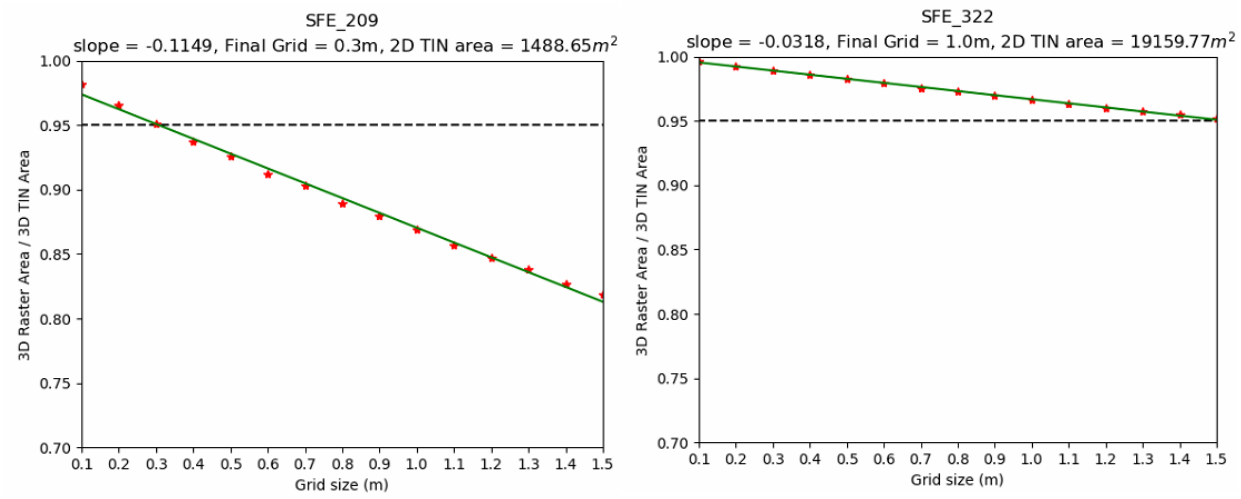

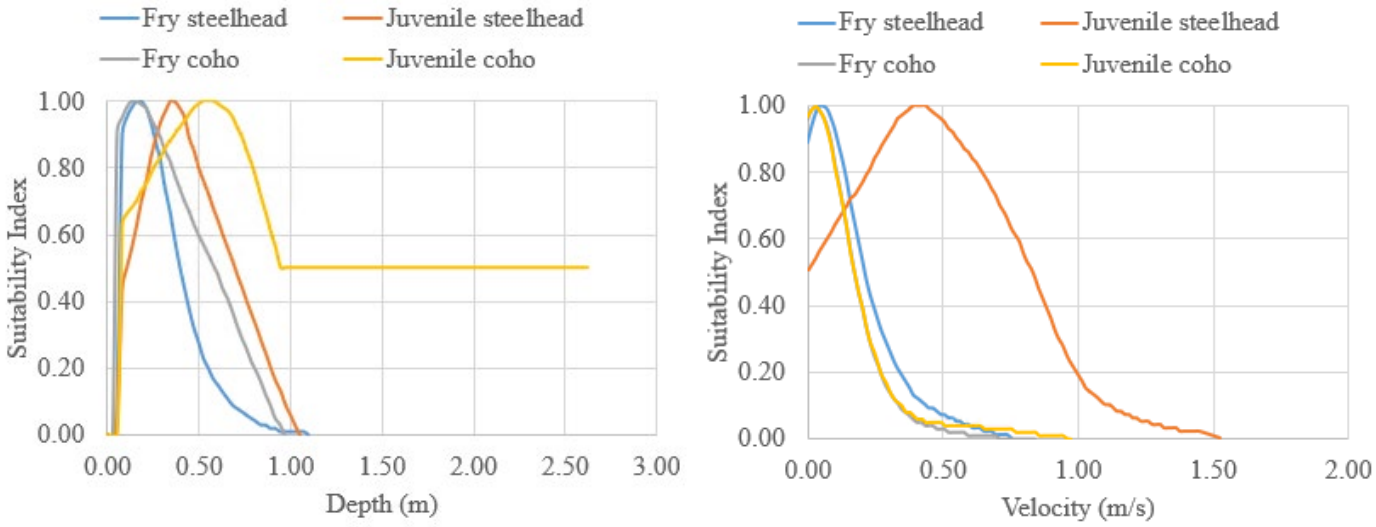

Figure S5. Habitat suitability curves for velocity and depth for fry/juvenile Steelhead trout and Coho salmon. These HSCs were generated based on fish use and habitat availability data collected from June 2017 to 2018 and the sample size for each fish species and lifestage ranges were 575 (Fry steelhead), 1,555 (Juvenile steelhead), 638 (Fry coho), and 786 (Juvenile coho), respectively. We employed Category III HSCs (sensu Nestler et al., 2019) accounting for forage ratio correcting bias associated with habitat availability.

Synthetic terrains

Classified as a "Confined, gravel-boulder, high width-to-depth, riffle-pool" channel, SFE 322 showed non-uniform geomorphic characteristic affecting vertical variation of topography such as a center bar at the entrance, a riffle-pool sequence, and large substrate particles spread around the riffle and sidebars (Figure S6a, baseline scenario). The synthetic channel scenario with thalweg bed undulation, *s2*, was able to capture the pool-riffle sequence whereas other synthetic channels could not (Figure S6a, synthetic terrain). For SFE 322, the transect lines were at the crest or trough of riffle (0), pool (1), riffle (2), and pool (3). For the baseline scenario, the cross-section was trapezoidal at riffles (0, 2), symmetric V-shape at the first pool (1), and asymmetric V-shape at the second pool (3). In addition, we observed the roughness elements were placed at the riffles (0, 2). For synthetic channel, the cross-sectional shape at all cross sections were similar to that of baseline scenario except for the first pool.

Site SFE 25 is characterized by width expansion and contraction of the channel (Figure S6b, baseline scenario) and such width variability is well represented in scenario *s1*. The transect lines were placed where expansion/contraction was observed and at the end of the channel. Cross sections of surveyed and synthesized channels were well matched except for the transect, 0. At the first transect, point bars are observed which potentially split water flow and this lateral channel variability was not captured by River Builder.

Site SFE 209 exemplifies the "Confined, high-gradient, cobble-boulder, cascade/step-pool" channel type which is prevalent in mountain valleys (Figure S6c). Large boulders were placed across the floodplain (Figure S6c, baseline scenario) and scenario *s0* with bed roughness was able to mimic these features (Figure S6c, synthetic terrain). The synthetic terrain reproduced the cross-sectional profile and random roughness structures on bed in synthetic terrain.

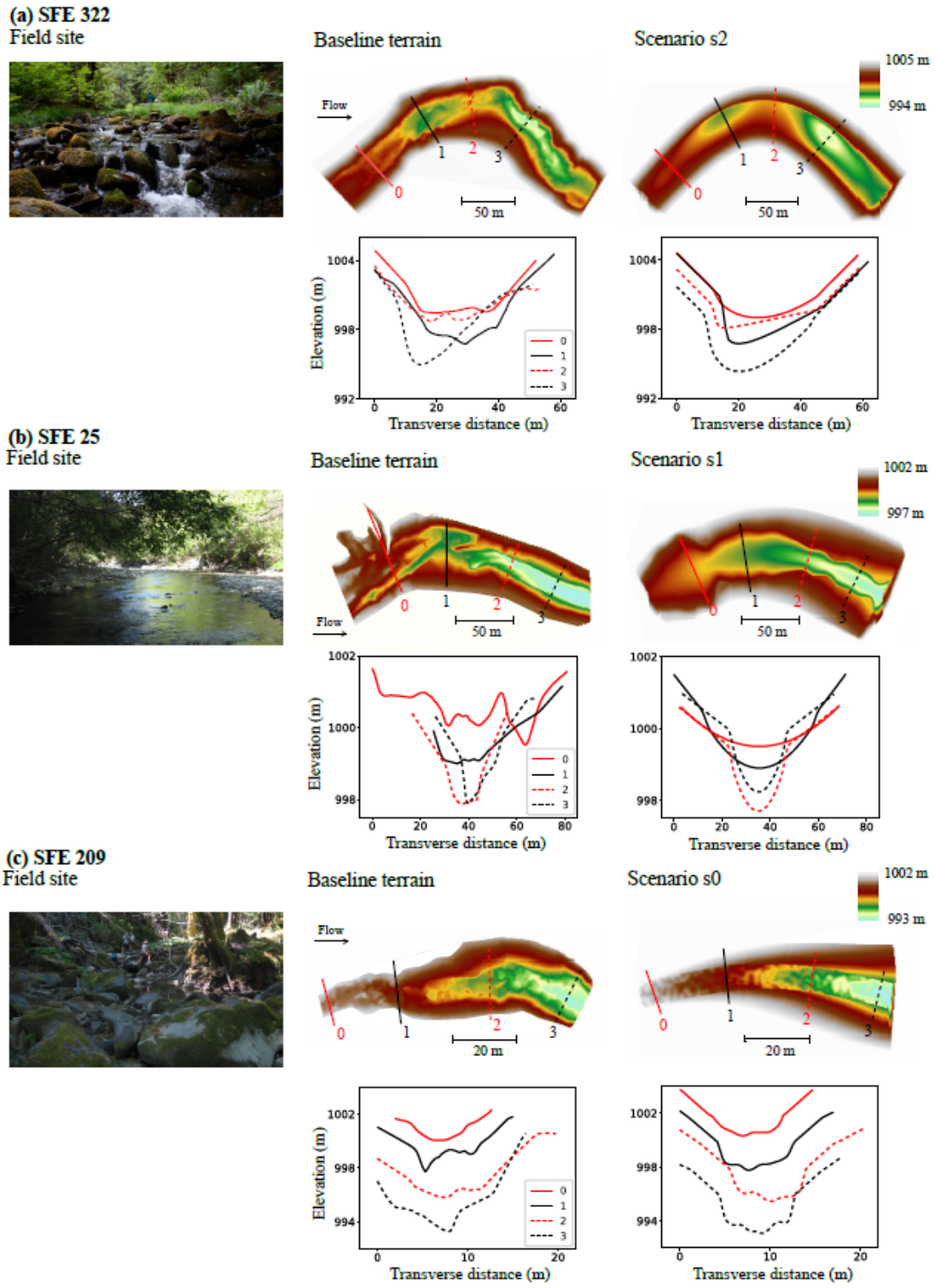

Figure S6. Representative photos of the field site, 3D channel topography, and cross-sectional profiles (0-Solid red, 1-Solid black, 2-Dotted red, 3-Dotted black) of the baseline (left) and synthetic (right) channel scenarios with dominant channel variability functions for (a) SFE 322, (b) SFE 25, and (c) SFE 209

Table S2. A summary table of hydraulic test metrics, Kullback-Leibler Divergence (KLD) values, and their average values for each channel scenario for each flow variable, depth or velocity. The scenario with smallest KLD is highlighted in grey.

Flow condition	Flow variable	Site ID	*n0*	*s0*	*s1*	*s2*
Baseflow	Depth	SFE 322	20.174	14.809	20.193	2.256
		SFE 25	18.204	18.180	15.976	0.375
		SFE 209	5.192	0.295	5.235	0.332
		Average	14.523	11.095	13.801	0.988
	Velocity	SFE 322	2.260	1.159	2.443	0.278
		SFE 25	4.833	4.827	3.068	0.293
		SFE 209	2.423	0.038	2.115	0.310
		Average	3.172	2.008	2.542	0.294
Bankfull	Depth	SFE 322	5.010	3.512	3.431	0.398
		SFE 25	6.659	6.660	0.086	0.289
		SFE 209	3.469	0.224	2.646	0.421
		Average	5.046	3.465	2.054	0.369
	Velocity	SFE 322	0.762	0.535	0.474	0.406
		SFE 25	4.138	4.172	0.141	0.456
		SFE 209	0.468	0.189	0.517	0.212
		Average	1.789	1.632	0.377	0.358

References

Kalbermatten, M., Van De Ville, D., Turberg, P., Tuia, D., and Joost, S. (2012) Multiscale analysis of geomorphological and geological features in high resolution digital elevation models using the wavelet transform. Geomorphology, 138(1), p.352-363

Kuriyama, Y., and Yanagishima, S. (2016) Investigation of medium-term barred beach behavior using 28-year beach profile data and Rotated Empirical Orthogonal Function analysis. Geomorphology, 261, p.236-243.

Nestler, J.M., Milhous, R.T., Payne, T.R. and Smith, D.L. (2019). History and review of the habitat suitability criteria curve in applied aquatic ecology. River Research and Applications, 35(8), 1155-1180.